The investigation of influence of tool wear on ductile to brittle transition in single point diamond turning of silicon

Amir Mir[a], Xichun Luo[a], Jining Sun[b]

[a]Centre for Precision Manufacturing, Department of Design, Manufacture and Engineering Management, University of Strathclyde, Glasgow, U.K

[b]School of Engineering & Physical Sciences; Heriot-Watt University, Edinburgh, U.K

Xichun.luo@strath.ac.uk

Abstract

Single point diamond turning (SPDT) of large functional surfaces on silicon remains a challenge owing to severe diamond tool wear. Recently, tremendous efforts have been made in understanding the machining mechanics, especially wear mechanism of diamond tools in SPDT of silicon. However, the localized transition of machining mode from ductile to brittle as a result of progressive tool wear has not been well understood yet. In this paper both experimental and numerical simulation studies of SPDT were performed in an effort to reveal the underlying phenomenon of ductile to brittle transition (DBT) as a consequence of diamond tool wear. Series of facing and plunging cuts were performed and the profile of machined surface was evaluated together with the progression of tool wear. The transition stages from ductile to brittle were identified by analysing the surface profiles of plunging cuts using a scanning electron microscope (SEM) and a 2D contact profilometer and a white light interferometer. The progressive degradation of the cutting edge of diamond tool and its wear mechanism was determined using Least Square (LS) arc analysis and SEM. The study reveals that at initial tool wear stage, the ductile to brittle transition initiates with the formation of lateral cracks which are transformed into brittle pitting damage with further tool edge degradation. Numerical simulation investigation using smoothed particle hydrodynamics (SPH) was also conducted in this paper in order to gain further

insight of variation of stress on the cutting edge due to tool wear and its influence on brittle to ductile transition. A significant variation in frictional resistance to shear deformation as well as position shift of the maximum stress values was observed for the worn tools. The magnitude and distribution of hydrostatic stress were also found to change significantly along the cutting edge of new and worn diamond tools.

Keywords: diamond turning, silicon, tool wear, SPH, ductile to brittle transition

1. Introduction

Silicon is one of the most-preferred materials in weight-sensitive infrared applications and micro-photonics applications due to its desired characteristics of high refractive index, low mass density, and low thermal expansion coefficient. The performance of silicon-based functional surfaces is highly reliant on high form accuracy and optical surface quality. However, machining of silicon is a complex process due to material anisotropy and its pressure-sensitive characteristics which are highly dependent on varying tool-workpiece interface conditions. Single point diamond turning (SPDT) process has emerged as one of the most efficient ultra-precision manufacturing methods to fabricate products with nanometric surface finish. The elastic-plastic deformation of silicon can be achieved in SPDT process by utilizing brittle to ductile transition (BDT) phenomenon. The notion of BDT attributed to high-pressure phase transformation (HPPT) as a function of tool geometry and controlled material removal conditions [1-3]. Due to the high hardness of silicon, diamond tool experience severe wear which change the localized conditions for BDT in the chip formation zone and silicon endures brittle fracture eventually.

Due to difficulty in observation or measurement in machining, experimental and simulation studies of indentation [4-9] and scratch test [10-13] have frequently been

conducted to understand the localized material response behaviour of silicon under machining conditions. The brittle fracture of silicon in these studies is attributed to crack formation during loading and unloading processes. Radial, median, lateral, half-penny and quarter-penny cracks have been found to emerge in indentation and scratch test studies of silicon [8, 11, 14]. Structural phase transformation of silicon as well as crack type and geometry, and crack propagation directions significantly change due to the variation in loading and unloading conditions [9, 15-18]. Although, indentation and scratch test studies provide useful insight of machining mechanism of silicon, the tool geometry, loading and unloading conditions and material removal contour in these studies are significantly different from those occurring in machining processes. Also, the influence of tool wear (imperfection, defect, or wear of stylus) on material deformation behaviour is not considered in these studies.

In diamond turning, the ductile and brittle behaviour of silicon as a function of tool geometry and machining conditions was first presented by Blake and Scattergood [1]. They proposed critical chip thickness criteria for BDT as a function of tool geometry, feed rate and depth of cut. Based on critical chip thickness criteria and other investigation studies of diamond turning [1, 19-22], when right tool geometry and cutting parameters are used, diamond turning of silicon can be achieved in ductile mode.

Regardless of choosing right tool geometry and machining conditions, diamond tool wear still remains an ultimate criterion that governs plastic deformation or brittle fracture [21, 23, 24]. In SPDT of silicon, the wear of diamond tool facilitates brittle fracture which in turn offers high cutting resistance to diamond tool promoting further tool wear. In order to prolong the ductile mode machining, it is crucial to understand

the material removal mechanism during ductile to brittle transition (DBT) as a function of progressive tool wear.

The progressive and final tool wear pattern and mechanism, as well as its influence on the plastic deformation and brittle fracture of silicon during plunging cut, are analysed in this paper. In addition, a numerical simulation study using Smoothed particle hydrodynamics (SPH) approach is performed to investigate the influence of progressive tool wear on the machining mode and distribution of stresses on the machined surface along the cutting edge of the diamond tool.

2. Experimental study

Diamond turning experiments were carried out on an ultraprecision diamond turning machine (Moore Nanotech 250UPL) which possesses an air bearing work spindle and hydrostatic motional slides. Single crystal diamond tools with dodecahedral orientation were used in the experiment. A number of facing cuts were performed on the (111) surface of single crystal silicon until onset of brittle fracture on the machined surface. Each facing cut covered an average cutting distance of 5 km. Before the first facing cut the diamond tool was plunged into the silicon surface at a distance of 6 mm to its centre to record the tool profile of the new diamond tool. Plunging cuts were performed after each iteration of facing cut to obtain progressive tool wear contour. Fig. 1 presents machining scheme of the facing and plunging cuts adopted in this study. Details of workpiece, tool geometry and machining conditions are presented in Table 1.

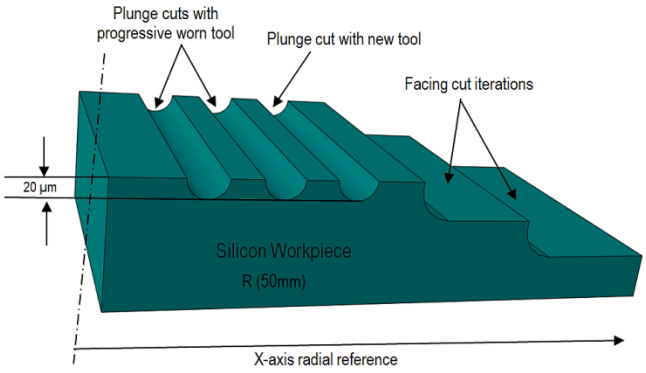

Fig. 1: Experimental SPDT plan details

The cutting forces during facing and plunging cuts were measured by a Kistler dynamometer (9256C2). The machined silicon surface and plunge cuts were analysed using a 2D surface profiler (Taylor Hobson PGI 1240), a white light interferometer (Zygo Newview 5000) and an SEM (FEI Quanta 3D FEG) to study the material removal mechanics of silicon and diamond tool wear.

Table 1: Plunging cut experimental data and conditions

Silicon wafer	Diamond tools	Cutting parameters
Optical grade silicon, polished Round Orientation = <111> +/-5° Diameter = 100 mm Thickness = 5 mm Sample purity = 99.999%	Orientation = dodecahedral Rake angle = -25° Clearance angle: 10° Nose radius = 5 mm	Spindle speed =1200 rpm Cross-feed = 1 µm/rev In-feed = 0.1 µm/rev Depth of facing cut = 10 µm Depth of plunge cut = 20 µm Coolant = water mist

3. Results and discussion

3.1. Measurement of tool wear in machining trials

Different dominant tool wear mechanisms have been reported in previous studies on diamond turning of silicon. These wear mechanisms include thermo-chemical wear [25], abrasive wear due to formation of dynamic hard particles or diamond-like carbon particles [26-29], and abrasive wear due to the formation of silicon carbide (SiC) [29, 30]. The formation of hard particles has been attributed to phase transformation of

silicon from monocrystalline to amorphous phase consisting of group of atoms with shorter bond length. While, the formation of SiC or diamond-like carbon particles caused by diffusion of carbons of diamond tools into silicon at high temperature and high hydrostatic pressure [29].

The new diamond tool was examined using the SEM for any existing damage on the cutting edge and on the rake and flank faces of the tool prior to machining. Fig. 2(a) shows SEM image of the new diamond tool which indicate a very sharp cutting edge between the rake face and flank face. In SPDT of silicon, diamond tools get worn even after machining a short cutting distance. This can be observed in Fig. 2(b) which shows thin groove marks appeared on the flank face of diamond tool after cutting distance of 5 km. The groove wear depth further increases with increasing cutting distance. The maximum flank wear width of 7 μm was observed on the main cutting edge side reducing towards the apex of the tool and further to the trailing edge. In cross-feed motion, when the tool approaches silicon workpiece, the main cutting edge comes in contact with the workpiece surface followed by the apex of the tool and subsequently trailing edge. The maximum stresses develop at the main cutting edge due to cutting maximum chip thickness which reduces towards the apex of the tool [1]. Hence high flank wear occurs towards the main cutting edge compared to apex and trailing edge. Abrasive wear mechanism was found dominant in the form of frictional groove wear as shown in Fig. 2(c) and 2(d). In order to investigate the formation of SiC (which may possibly be the cause of abrasion, if present), Energy-dispersive X-ray spectroscopy (EDX) was performed on the chips collected during ductile as well as brittle mode machining. In the EDX analysis, no traces of SiC were detected in ductile and brittle chips. The groove wear on the flank face of diamond tool can

therefore be attributed to the formation of dynamic hard particles due to the phase transformation of silicon at high hydrostatic pressure.

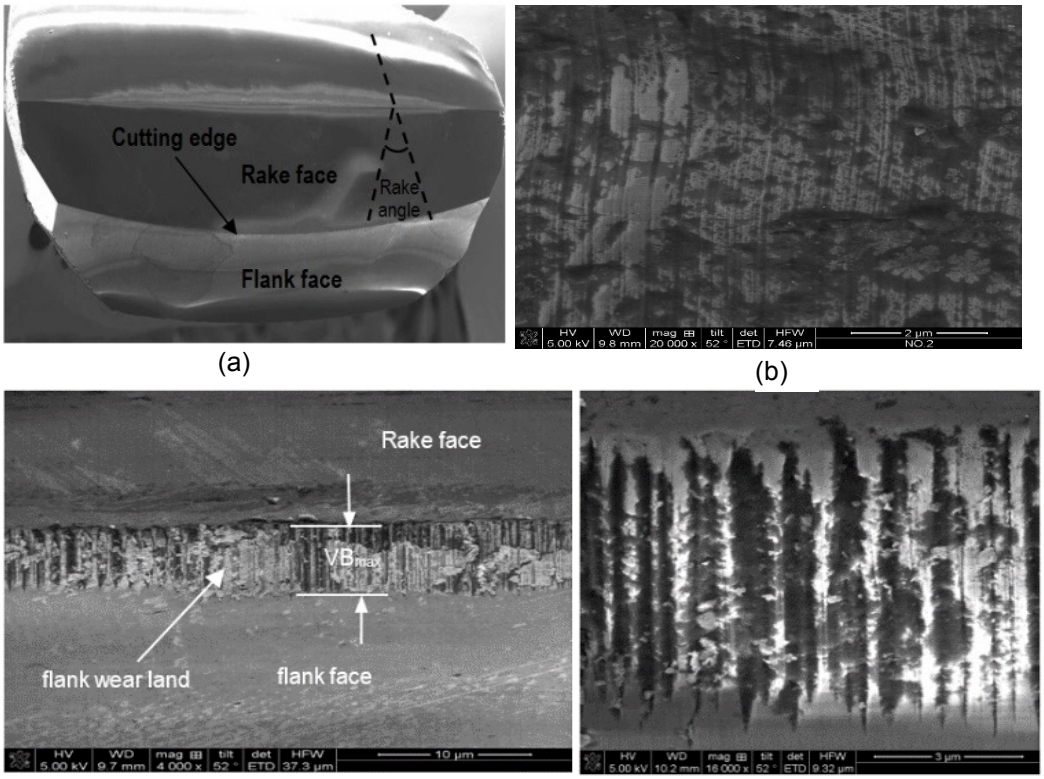

Fig.2: SEM images of diamond tool (a) new tool (b) flank wear (after cutting distance of 5 km) (c) Final tool wear when brittle fracture appeared on silicon surface (d) zoomed image of (c) shows groove and abrasive wear mechanism

Fig. 3 shows the schematic illustration of the degradation of tool radius and profile of the plunging cut of the diamond tool after 5 km of cutting distance.

The Least Square (LS) arc analysis [21] of the plunge profile by the worn diamond tool was performed to obtain the tool edge recession. Basically the analysis regards the plunge profile by the trailing edge as a datum (due to less wear on that side) and to LS fit it with the main cutting edge profile to obtain the whole wear area as shown in Fig. 4. The wear area was calculated using the following relation:

$$w_a = (P_a \times P_{Lo}) - (P_{aN} \times P_{LoN}) - - - -(1)$$

Where P_a is the average height and P_{Lo} is the profile length of the modified profile in LS arc analysis method. They represent the average recession of round edge of the tool and increase in contact width respectively. The parameters P_{aN} and P_{LoN} are the average height and length of the new tool edge profile. The approximate recession of the rake face (w_{aR}) of the tool with the rake angle (α) can then be calculated by using following equation:

$$w_{aR} = w_a/cos\alpha \quad ----(2)$$

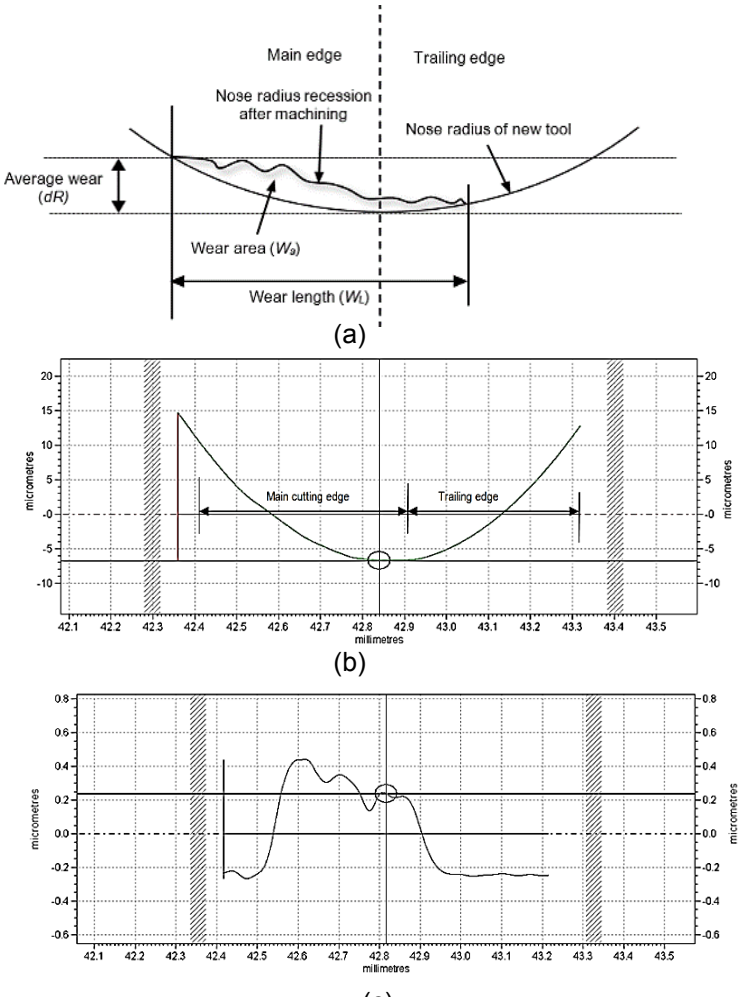

Fig. 3: Estimation of tool wear (a) schematic illustration of the tool edge recession (b) Plunge profile of worn tool after 5 km (c) Zoomed-in image showing worn area of the main cutting edge

Fig. 4 shows the result of LS arc analysis [21] of tool plunge profiles, i.e. the recession of tool along the cutting edge on the rake face after cutting distances of 15 km, 30 km and 40 km. A significant increase in the average tool recession can be observed from cutting distances from 15 km to 40 km.

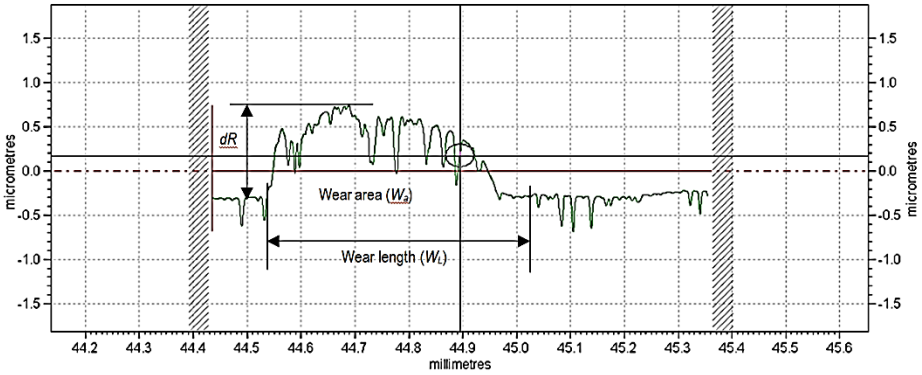

(After 15 km)

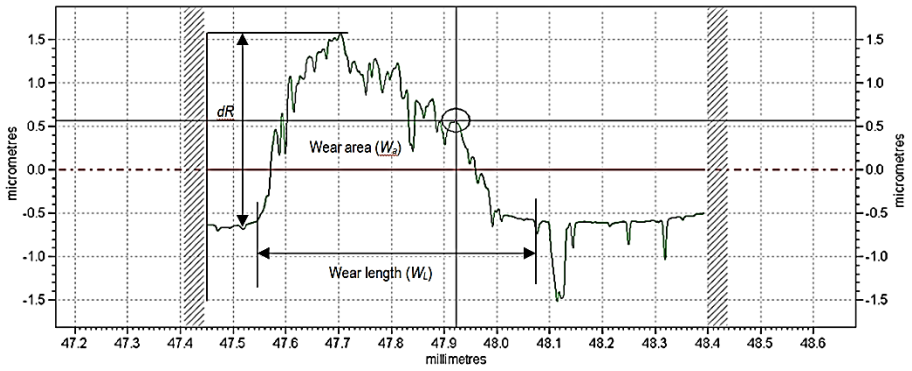

(After 30 km)

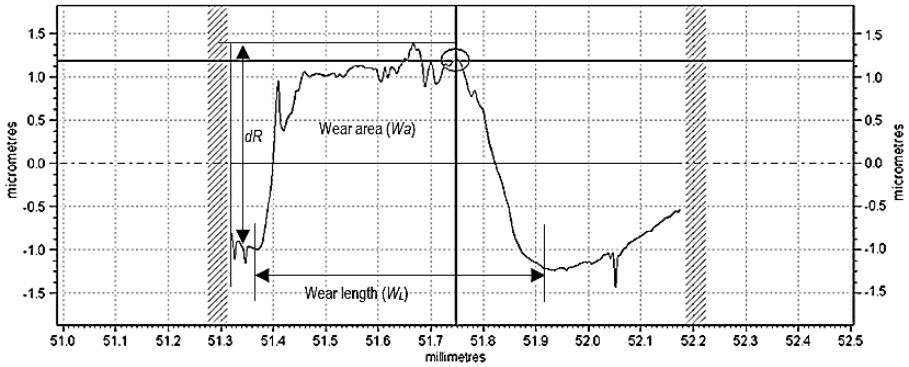

(After 40 km)

Fig. 4: LS arc analysis to measure edge recession of diamond tool

Fig. 5 shows the progression of tool wear area with the increasing cutting distance and the variation of average cutting forces during face turning and plunging cuts. With the increase of the cutting distance, tool wear area as well as the magnitude of cutting forces increases. A sharp increase of the tool wear rate was found during initial cuts (between cutting distances of 5 km and10 km). Tool wear rate showed steady behaviour during middle phase (cutting distances from 10 km to 25 km), and endured severe tool edge degradation after cutting distance of 30 km until the onset of brittle fracture. The higher tool wear rate during the initial cuts attributed to a general trend of quick edge recession of sharp cutting edges. The tool maintains its strength and tool edge degrade with the lower wear rate during the middle phase. With the increase in brittle fracture of silicon, the frictional resistance increases, and the tool undergoes severe abrasive wear in the final phase. A good correlation of the tool wear area and tangential and thrust forces can be observed in Fig. 5. The contact pressure between the tool and the workpiece drops with the tool edge recession since the input depth of cut (z-axis travel) for all plunge cuts remains the same. However, frictional resistance between the tool and the workpiece increases with the dullness of the diamond tool and hence increase of cutting forces. The reduction in tangential and thrust forces in the final phase of facing cut attributed to the superimposition of effect of contact pressure reduction over frictional resistance with further edge degradation. In plunging cut, due to full tool edge contact, the frictional resistance superimposes the effect of contact pressure reduction and hence the cutting forces continuously increase until the onset of brittle fracture on the silicon surface.

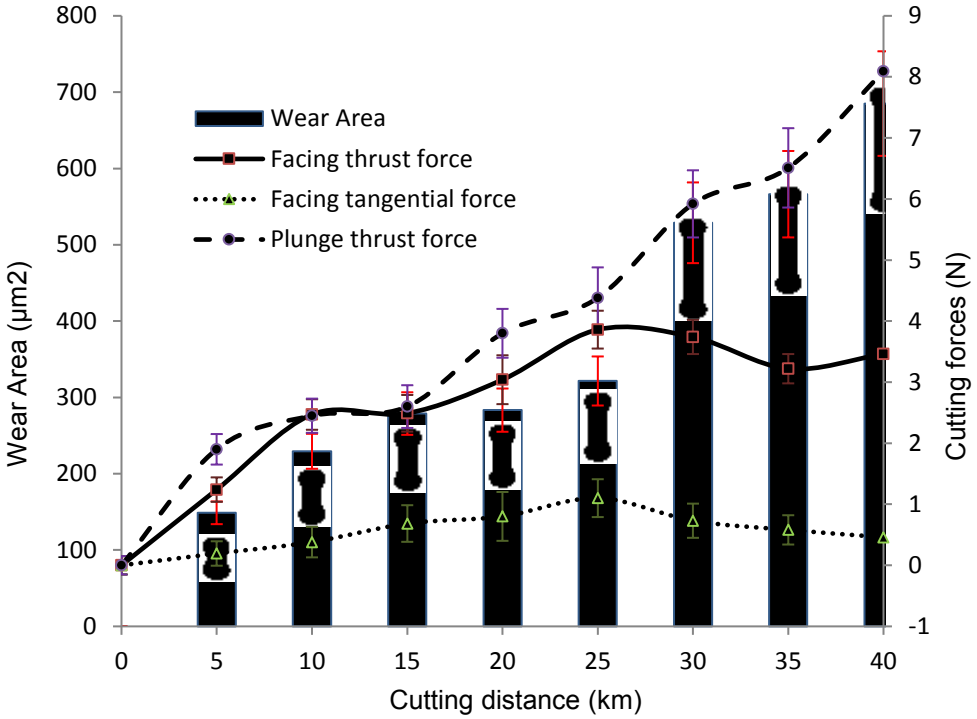

Fig. 5: Progression of tool wear and cutting and thrust forces trend with the increasing cutting distance

3.2. Ductile to brittle transition

The machined surfaces of silicon obtained by plunging cut were observed by SEM. The transition of machining mode from ductile to brittle fracture can be observed with the formulation of lateral cracks along with the ploughing marks leading to brittle removal of material. Series of lateral cracks appeared across the tool path in the initial stage of tool wear at 15 km as shown in Fig. 6(a). They propagated deep into the surface at 25 km (Fig. 6(b)) with further wear and ensued into severe brittle damage at 35 km as shown in Fig. 6(c). The initiation of lateral cracks can be attributed to the local uneven stress distribution along the tool path due to unloading and tool wear. When the tool cutting edge is sharp, it remains in contact with the machined surface; and due to high cutting speed, unloading phenomenon doesn't transpire completely. However, when the tool edge degrades, the irregular unloading occurs across and parallel to the tool path dependent on the wear contour. The local tensile stress develops behind the tool cutting edge during unloading in contrast to compressive

stress in front of the cutting edge. When the stress difference is small, lateral cracks appear but brittle damage doesn't occur completely as was observed in Fig. 6(a). With the increase of difference in pressure (at surfaces *a* & *b* in Fig. 6(b)), the surfaces (*a & b*) overlaps. Material removal through brittle fracture occurs in the next stage 3 (Fig. 6(c)) with further pressure difference due to high tool wear.

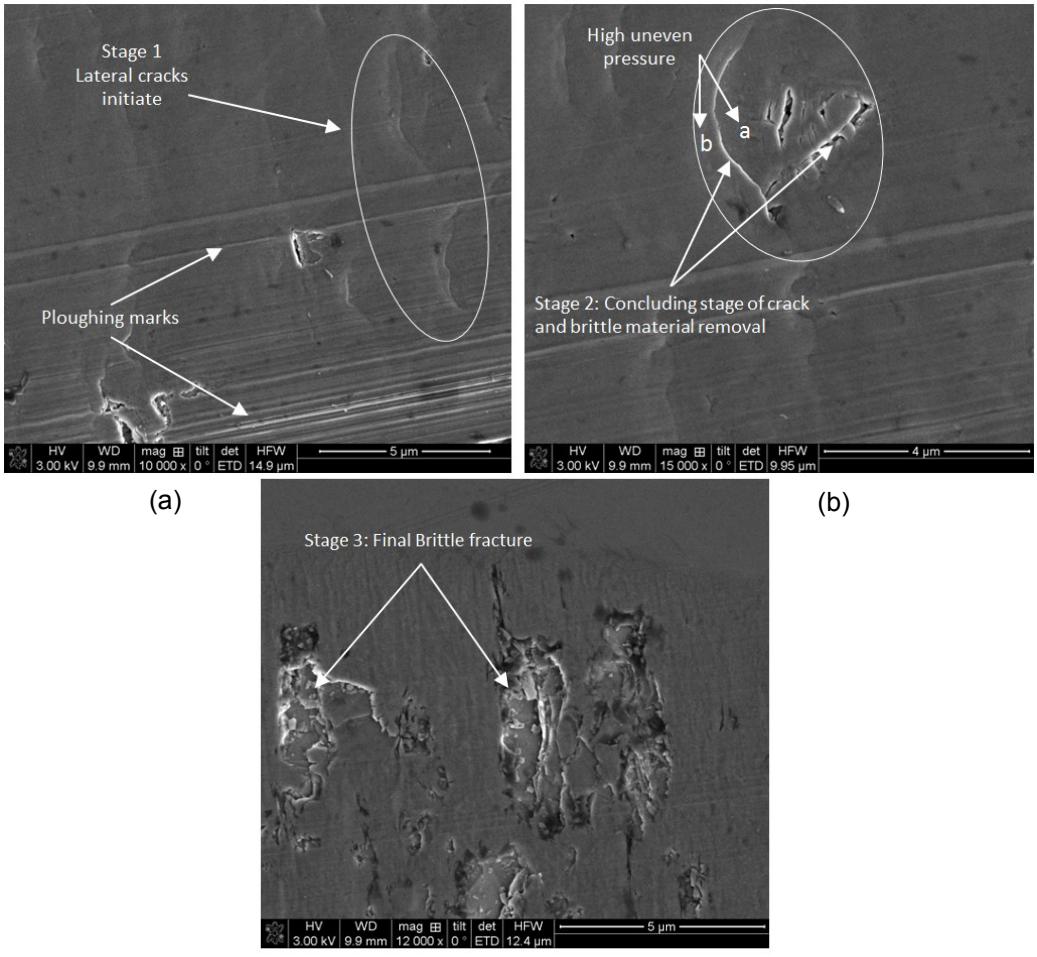

Fig. 6: Surface damage and lateral cracks from (a) crack initiation stage (b) crack concluding stage (c) brittle material removal

It is important to note that these lateral cracks and fracture were more severe in the middle and main cutting edge side. The analysis of brittle fracture in the plunging cut area suggests that mild ploughing occurs with frictional tool edge degradation,

promoting lateral cracks to initiate first followed by the median cracks. The material removal along the edges was also found to occur due to the lateral crack turned into the chipping damage propagating into the optical smooth machined surface area as shown in Fig. 7.

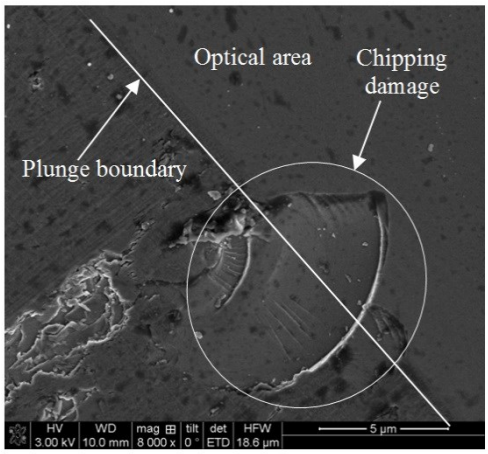

Fig. 7: chipping along plunge boundary propagating into optical area

3.3. Plunge surface measurement

The machined surfaces topography obtained by plunging cuts were also analysed by using white light interferometry. The plunge profile geometry as well as surface topograhpy in the final plunging cut can be observed in Fig. 8. The depth as well as the width of the plunge cut was found to reduce due to increasing tool wear.

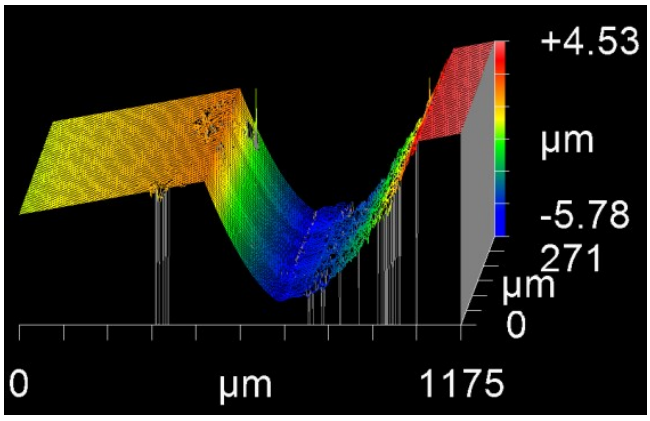

Fig.8: Plunge cut surface with final brittle fracture

The brittle fracture damage on the plunge surfaces was found to increase with the progressive tool wear, so did the surface roughness (R_a). Fig. 9 presents the variation in plunge width as well as surface roughness with the increasing tool wear area. The maximum reduction in width was observed during phase 1. During phase 2, the plunge width remain stable with slight variation, and then sharply reduced in the final phase until the onset of brittle fracture.

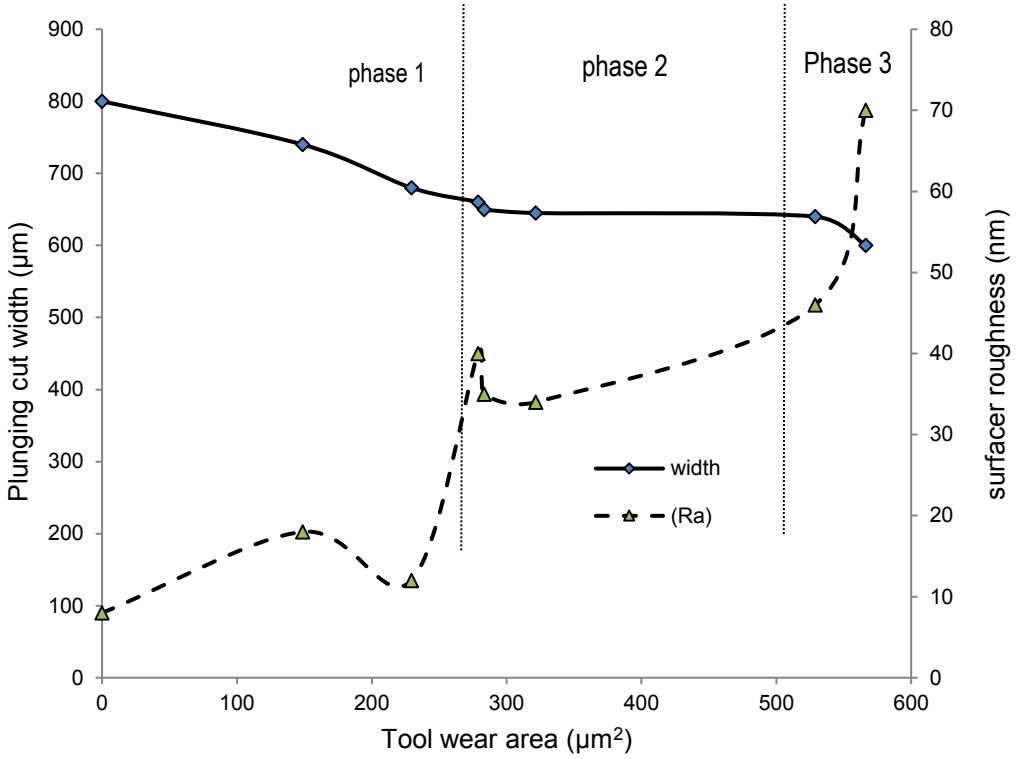

Fig. 9: Variation of plunging cut width and surface roughness with tool wear

The surface topography of the initial and final plunge cuts was presented in Fig. 10. During facing cuts, the maximum tool wear occurs at the main cutting edge of the tool. When plunging cuts are performed with a worn tool, the tool cutting edge condition governs the machining mechanism developed during the plunging cut. Due to main cutting edge wear during face turning, the material removal in the plunging cut was achieved by brittle fracture on the main cutting edge side. A better

surface roughness can be observed on the trailing edge side in the plunging cut. The reduction in tool-workpiece contact width was also recorded from 800 µm to 580 µm in the initial and final plunge cuts respectively.

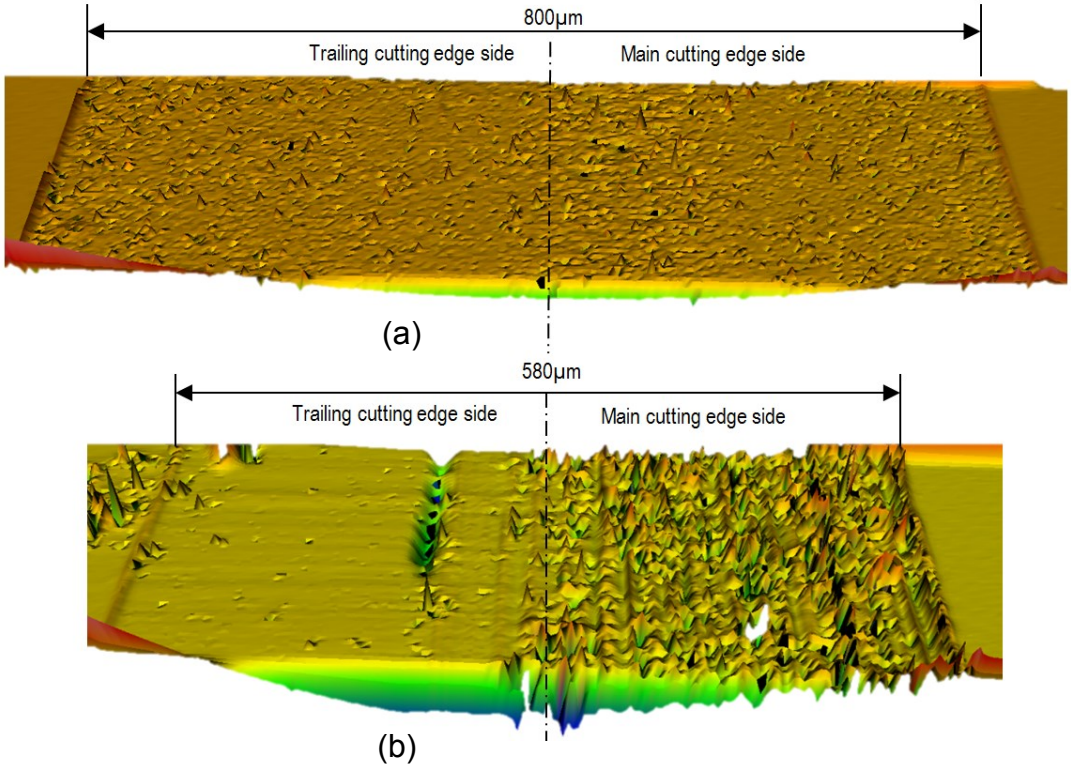

Fig. 10: Surface topography of (a) initial plunge cut and (b) final plunge cut

4. SPH machining model

In experimental study, the localized chip formation and stress distribution in the chip formation zone and any change with the progressive tool wear cannot be truly determined. A numerical study using SPH approach was performed to address these experimental limitations. Compared to classical Lagrangian mesh-based method, the SPH approach eliminates the high mesh distortion issue without defining chip separation or remeshing criteria.

4.1. SPH kernel approximation

SPH uses kernel approximation to approximate field variables and properties in the SPH solution domain as shown in Fig. 11. SPH approximate field variables at any particle by classical summation of smoothing function values of neighbouring particles within a sphere of influence. The length of the sphere of influence is defined as the maximum distance to which the interaction can occur.

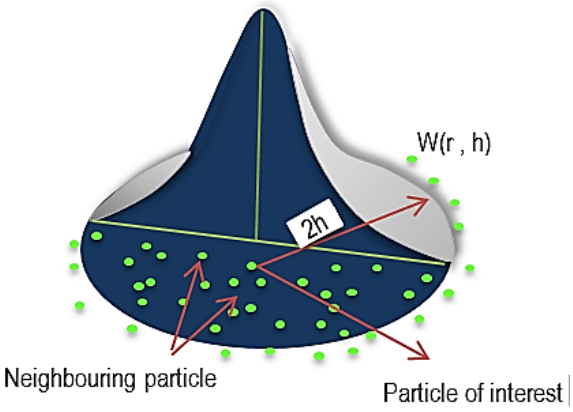

Fig. 11: SPH kernel approximation

The SPH approximation is derived from the following equation:

$$f(x) = \int_V f(\acute{x})\delta\,(x - \acute{x})\mathrm{d}\acute{x} - - - - \quad (3)$$

Where $f(x)$ is a scalar function of the three-dimensional position vector *x* ranging within a volume *V*. $\delta(x - \acute{x})$ is the Dirac's delta function. The kernel is normalized to unity as below:

$$\int_V W(x - \acute{x}, h)\mathrm{d}\acute{x} = 1 - - - - (4)$$

When *h* approaches zero, the smoothing kernel will satisfy the delta function

$$\lim_{h\to 0} W(x - \acute{x}, h) = \delta(x - \acute{x}) - - - - \quad (5)$$

So the scalar function $f(x)$ in with the kernel function *W* can be described as

$$f(x) = \int_V f(\acute{x}) W(x - \acute{x}, h)\, \mathrm{d}\acute{x} \quad ----- (6)$$

The function $f(\acute{x})$ can be deduced by considering the kernel in the form of point spread function. In the discrete SPH form, the values of $\acute{x}$ turns into the set of SPH particle's discrete position and the summation function replace the integral. The SPH particle approximation can finally be written as

$$f(x) \cong \sum_{j}^{\mathrm{n}} \frac{(m_j)}{\rho_j} f(x_j) W\left(|x_i - x_j|, h\right) ----- (7)$$

Where $f(x_j)$ is the scalar value of *j-th* particle and m_j and ρ_j are the mass and densities of *j-th* particles; where *j* represents the neighbouring particle of the *i-th* particle for which field variables need to be approximated.

4.2. SPH machining model

A three-dimensional SPH diamond turning process model was developed by using general-purpose finite element software Abaqus. In order to study the influence of groove wear on material removal mechanism of silicon, plunging cuts were performed using new as well as worn diamond tools with groove flank wear. A similar groove tool wear contour observed in machining experiment by SEM was modelled with two different length of flank wear. Fig. 12 illustrates the new and worn diamond tools models adopted in SPH simulation study of silicon.

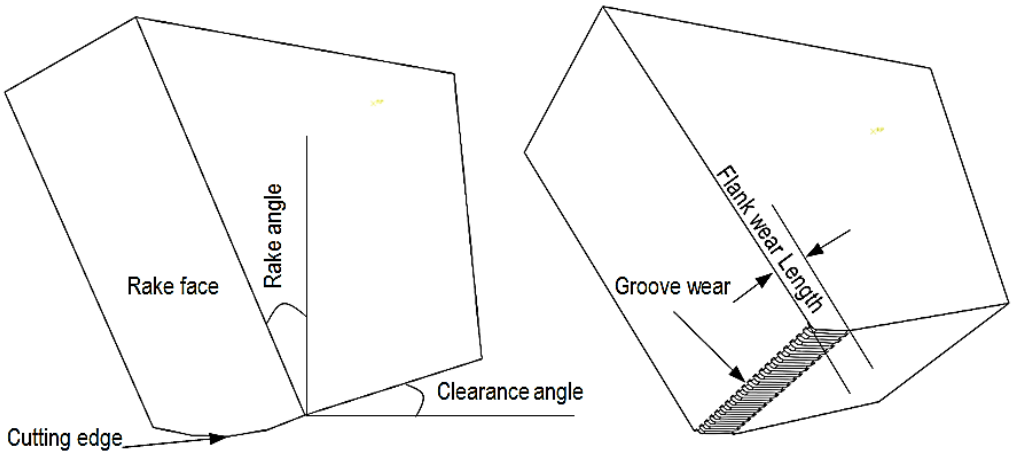

Fig. 12: Diamond tool models in SPH study: new tool (left) and worn tool (right)

The SPH machining model of silicon with geometry and boundary conditions are presented in Fig. 13. The diamond tool was considered as a rigid body and modelled with Lagrangian mesh. The motion of the tool was constrained in the Y and Z directions. The velocity was assigned to the tool in the negative-x direction to obtain chip formation. The silicon workpiece was modelled as a deformable part consisting of SPH particles. The bottom surface nodes of silicon workpiece were fixed with encastre conditions to restrict the motion of the workpiece in all directions. The walls of the workpiece were constrained in the z-direction to achieve required material stiffness during chip formation.

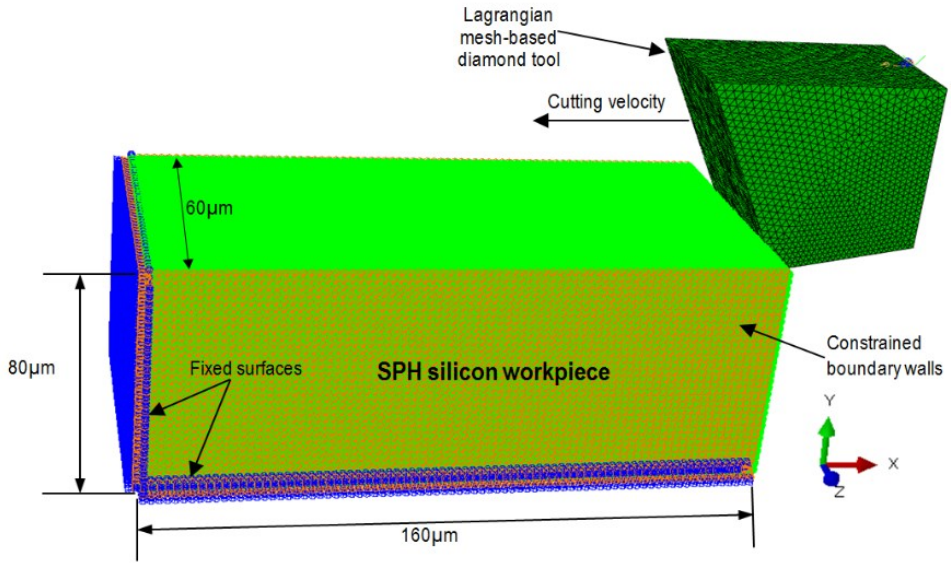

Fig. 13: SPH machining model of SPDT of silicon

Since all SPH particles in contact with the cutting tool are influenced by their neighbouring particles, it is crucial to define the nodal coordinates of these particles uniformly distributed in all directions. The sweep technique with medial axis mesh algorithm and minimized mesh transition features was adopted to produce the uniform mesh. The SPH particle density was selected based on convergence test study. The cutting parameters, tool and workpiece geometry adopted in the simulation study are detailed in Table 2.

Table 2: Cutting parameters used in SPH simulation

	Flank wear length (µm)	Rake/clearance angle	Workpiece dimensions (µm)	Cutting speed (m/s)	Depth of cut (µm)	SPH particles
Tool 1	0	-25°/10°	160x80x60	6.3	10	192580
Tool 2	4					
Tool 3	7					

Drucker-Prager (DP) model [31] was adopted as a material constitutive model to predict the deformation behaviour of silicon during SPH simulation. Unlike von Mises yield criterion, the DP model predicts the influence of the mean (hydrostatic) stress for

pressure-sensitive materials. The DP model has been frequently adopted for pressure-sensitive materials including concrete and rocks and has also been employed in machining of silicon nitride and silicon carbide [32]. One of the elementary criteria of using DP model is the higher compressive strength of pressure-sensitive material compared to its tensile strength. Silicon being a pressure-sensitive material with higher compressive strength compared to its tensile strength [33] satisfy the criteria. Table 3 lists the material and contact properties adopted in SPH simulation study.

Table 3: Material and contact properties during SPH simulation

Density, ρ	2330 kg/m^3
Elastic modulus, E	146 GPa
Poison's ratio	0.2
Friction coefficient	0.05
Friction angle (β)	26°
Dilation angle (Ψ)	20°
Flow stress ratio, k	0.82

4.3. Flank wear effect in SPH study

Cutting forces were calculated during simulations for the new and worn diamond tools. The SPH model was validated with experimental cutting forces. The thrust forces comparison of the new and worn diamond tools is presented in Fig. 14. Higher thrust forces were observed for the worn tools compared to the new diamond tool indicating an increase in cutting resistance with tool wear. Although forces during incipient stage of chip formation were found almost similar for both tools 2 and 3, for a significant period of cutting time, the forces observed for tool 2 with smaller flank wear were higher than tool 3 with higher flank wear. This behaviour can be attributed to a reduction in cutting energy due to reduced cutting depth with higher flank wear.

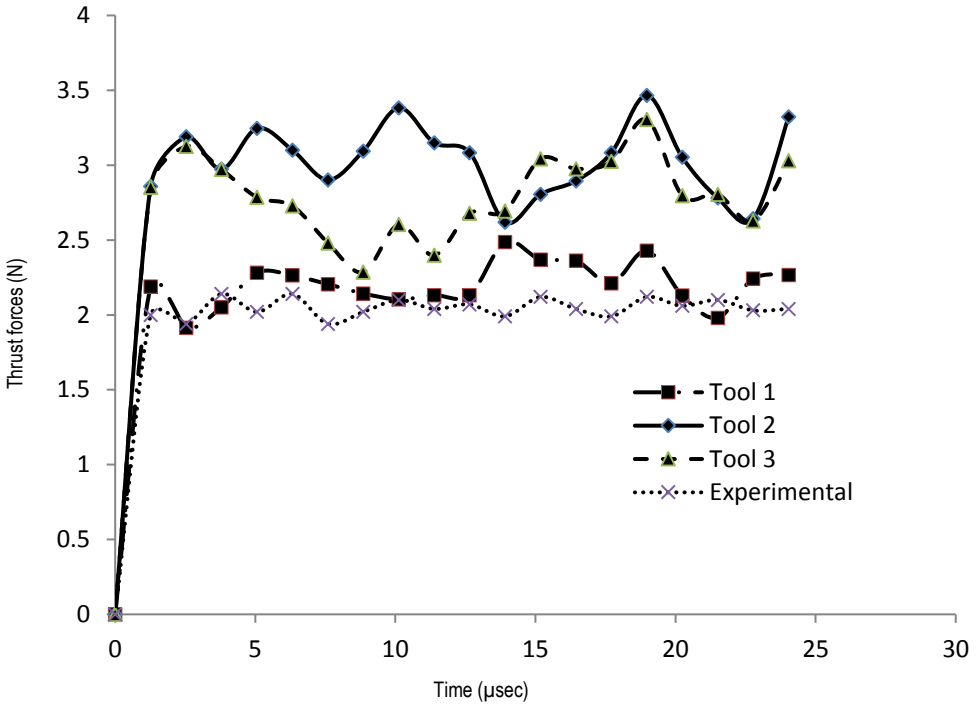

Fig. 14 : Thrust forces during SPH simulation with new and worn tools

Fig. 15 presents the von Mises stress distribution for the new and worn diamond tools. Von Mises stresses were observed significantly higher for the tool with lower flank wear width than the new as well as the tool with higher flank wear. For the new tool, the highest values of stresses were observed right underneath and in front of the cutting edge of the tool. However, when the tool is worn with the flank wear, the highest values of stresses were also observed right behind the worn edge of the tool. This behaviour exhibits a significant increase of frictional resistance to shear deformation due to rubbing of the flank worn area with the workpiece surface. For the worn tools, the offset distance of maximum values of stress from the main cutting edge is shown in Fig. 15. The displacements of maximum von Mises stress from the main cutting edge were measured as 4.6 μm and 7.4 μm for the tools with lower and higher flank wear width respectively. The maximum von Mises stress behind the worn edge

towards the machined surface surely contributes to the deterioration of machined surface as was observed in the experimental study.

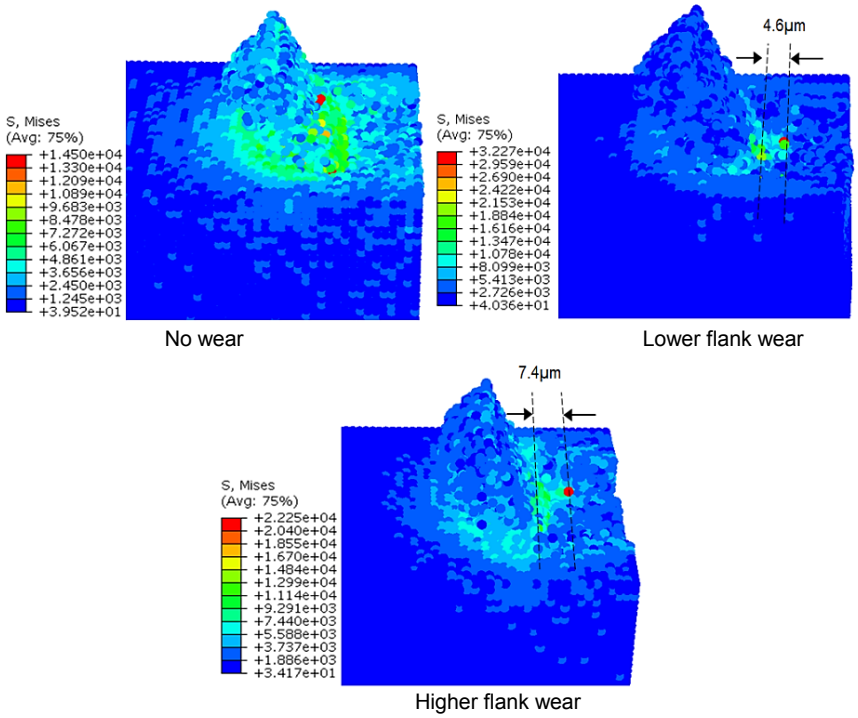

Fig.15 Von Mises stress (MPa) distribution for different tool wear conditions

With the tool wear, the shape of the cutting edge of the tool changes as shown in Fig. 16. The hydrostatic stress distribution on the machined surface along the cutting edge also varies with the change of tool-edge contour.

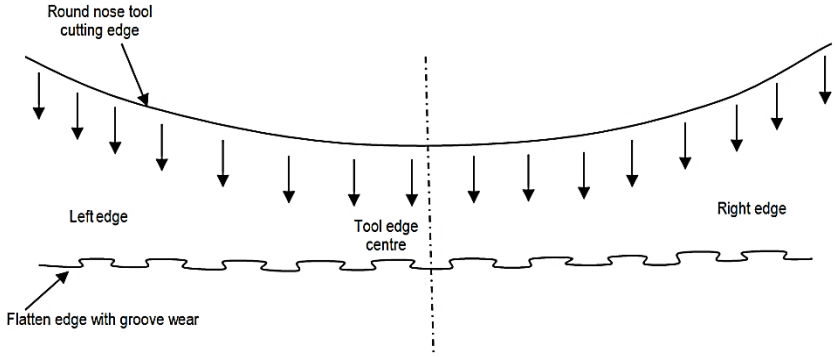

Fig.16: Schematic of tool edge variation from round to flat edge due to wear (arrows indicating hydrostatic pressure distribution)

Due to practical limitations in high-speed machining environment, it is difficult to identify the magnitude of global as well as localized hydrostatic pressure during cutting. During the simulations, the maximum hydrostatic pressure of 18 GPa, 32 GPa and 36 GPa was found in the plunge cut area for the tool 1, 2 and tool 3 respectively. The hydrostatic stress distribution in the plunge cut plane along the tool edge is presented in Fig. 17.

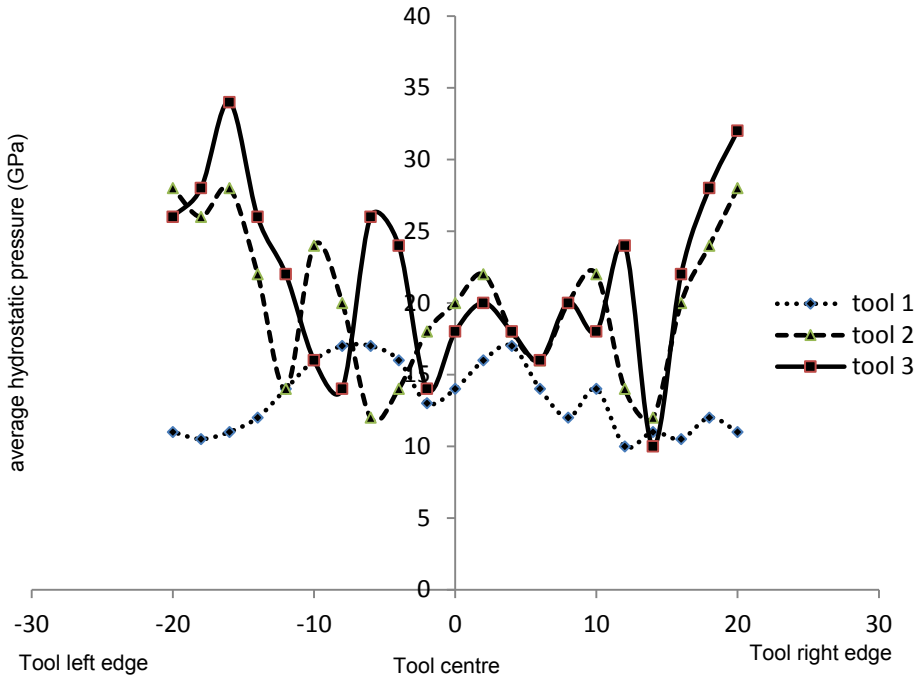

Fig. 17: Hydrostatic pressure distribution along the tool cutting edge

For the tool 1, the average hydrostatic pressure was found higher near the tool edge centre and reduced gradually towards the corners of the tool edge. However, for both tools 2 and 3, the average hydrostatic pressure was found increasing from the tool centre towards the corners of the tool edge on both sides. It was also noted that hydrostatic pressure between any two nearest positions fluctuate significantly for both tools 2 and 3, compared to the tool 1 for which the difference is much smaller. This

high pressure difference leads to lateral crack generation and results in onset of brittle fracture as observed in the experimental study by SEM.

5. Conclusions

Experimental and SPH based numerical simulation study were performed to investigate the influence of progressive diamond tool wear on material removal mechanics of silicon in SPDT. The correlative analyses of the tool wear profile and machined surface were performed. The conclusions are drawn as following:

- The transition of machining mode from ductile to brittle initiate with the formation of lateral crack at lower tool wear. It transforms into severe brittle damage with further increase of tool wear.
- For the sharp cutting edge, the location of maximum failure stress appears in front of the main cutting edge. With increasing flank wear length, the location of maximum failure stress displaces towards the machined surface behind the tool cutting edge, and it results in the deterioration of the machined surfaces.
- The hydrostatic stress distribution underneath the tool cutting edge significantly varies with the change of cutting edge contour. The high fluctuation of hydrostatic stress between the two nearest points, due to groove wear, facilitates the onset of brittle fracture on the machined surface.
- Since no traces of SiC were detected during the EDX analysis, groove wear on diamond tool is therefore, caused by the formation of hard particles. It supports the conclusions in Li and Cai's studies [27-28].

Acknowledgment

The authors gratefully acknowledge the financial support from the EPSRC (EP/K018345/1), Strathclyde University Impact Acceleration Account (120526/RA9029) and Royal Society-NSFC international exchange programme (IE141422) for this study.

References

1. Blake, P.N. and R.O. Scattergood, *Ductile-Regime Machining of Germanium and Silicon.* Journal of the American Ceramic Society, 1990. **73**(4): p. 949-957.
2. Goel, S.L., Xichun;Agrawal, Anupam;Reuben, Robert L., *Diamond machining of silicon: A review of advances in molecular dynamics simulation.* International Journal of Machine Tools and Manufacture, 2015. **88**: p. 131-164.
3. Jang, J.-i.L., M. J.;Wen, Songqing;Tsui, Ting Y.;Pharr, G. M., *Indentation-induced phase transformations in silicon: influences of load, rate and indenter angle on the transformation behavior.* Acta Materialia, 2005. **53**(6): p. 1759-1770.
4. Lawn, B. and R. Wilshaw, *Indentation Fracture - Principles and Applications.* Journal of Materials Science, 1975. **10**(6): p. 1049-1081.
5. Dietz, M. and H.D. Tietz, *Characterization of engineering ceramics by indentation methods.* J Mater Sci, 1990. **25**(8): p. 3731-3738.
6. Vodenitcharova, T., L.C. Zhang, and T.X. Yu, *Constitutive Modelling of Multi-Phase Transformation of Silicon under Nano-Scale Deformation.* Key Engineering Materials, 2003. **233-236**: p. 621-626.
7. Kim, D.E. and S.I. Oh, *Atomistic simulation of structural phase transformations in monocrystalline silicon induced by nanoindentation.* Nanotechnology, 2006. **17**(9): p. 2259-2265.
8. Wan, H.S., Yao;Chen, Qiulong;Chen, Youxing, *A plastic damage model for finite element analysis of cracking of silicon under indentation.* Journal of Materials Research, 2011. **25**(11): p. 2224-2237.
9. Jeong, S.-M.O., Han-Seog;Park, Sung-Eun;Lee, Hong-Lim, *Phase Transformation of Single Crystalline Silicon by Scratching.* Japanese Journal of Applied Physics, 2003. **42**(Part 1, No. 5A): p. 2773-2774.
10. Kailer, A., Y.G. Gogotsi, and K.G. Nickel, *Phase transformations of silicon caused by contact loading.* Journal of Applied Physics, 1997. **81**(7): p. 3057.
11. Vodenitcharova, T., O. Borrero-López, and M. Hoffman, *Mechanics prediction of the fracture pattern on scratching wafers of single crystal silicon.* Acta Materialia, 2012. **60**(11): p. 4448-4460.
12. Tseng, A.A.K., Chung-Feng Jeffrey;Jou, Shyankay;Nishimura, Shinya;Shirakashi, Jun-ichi, *Scratch direction and threshold force in nanoscale scratching using atomic force microscopes.* Applied Surface Science, 2011. **257**(22): p. 9243-9250.

13. Yoshino, M.A., T.;Shirakashi, T.;Komanduri, R., *Some experiments on the scratching of silicon.* International Journal of Mechanical Sciences, 2001. **43**(2): p. 335-347.
14. Luo, S.Y. and Z.W. Wang, *Studies of chipping mechanisms for dicing silicon wafers.* The International Journal of Advanced Manufacturing Technology, 2006. **35**(11-12): p. 1206-1218.
15. Juliano, T., Y. Gogotsi, and V. Domnich, *Effect of indentation unloading conditions on phase transformation induced events in silicon.* Journal of Materials Research, 2003. **18**(05): p. 1192-1201.
16. Juliano, T., V. Domnich, and Y. Gogotsi, *Examining pressure-induced phase transformations in silicon by spherical indentation and Raman spectroscopy: A statistical study.* Journal of Materials Research, 2011. **19**(10): p. 3099-3108.
17. Wasmer, K.B., C.;Gassilloud, R.;Pouvreau, C.;Rabe, R.;Michler, J.;Breguet, J. M.;Solletti, J. M.;Karimi, A.;Schulz, D., *Cleavage Fracture of Brittle Semiconductors from the Nanometre to the Centimetre Scale.* Advanced Engineering Materials, 2005. **7**(5): p. 309-317.
18. Haberl, B.B., J. E.;Swain, M. V.;Williams, J. S.;Munroe, P., *Phase transformations induced in relaxed amorphous silicon by indentation at room temperature.* Applied Physics Letters, 2004. **85**(23): p. 5559.
19. Shibata, T.F., Shigeru;Makino, Eiji;Ikeda, Masayuki, *Ductile-regime turning mechanism of single-crystal silicon.* Precision Engineering, 1996. **18**(2-3): p. 129-137.
20. Jasinevicius, R., Porto, A., Duduch, J., Pizani, P., Lanciotti Jr., F. and Santos, F. , *Multiple phases in silicon submicrometer chips removed by diamond turning.* J. Braz. Soc. Mech. Sci. & Eng., 2005. **27**(4): p. 440-448.
21. Durazo-Cardenas, I.S., P.;Luo, X.;Jacklin, T.;Impey, S. A.;Cox, A., *3D characterisation of tool wear whilst diamond turning silicon.* Wear, 2007. **262**(3-4): p. 340-349.
22. Chao, C.L.M., K. J.;Liu, D. S.;Bai, C. Y.;Shy, T. L., *Ductile behaviour in single-point diamond-turning of single-crystal silicon.* Journal of Materials Processing Technology, 2002. **127**(2): p. 187-190.
23. Uddin, M.S.S., K. H. W.;Li, X. P.;Rahman, M.;Liu, K., *Effect of crystallographic orientation on wear of diamond tools for nano-scale ductile cutting of silicon.* Wear, 2004. **257**(7-8): p. 751-759.
24. Uddin, M.S.S., K. H. W.;Rahman, M.;Li, X. P.;Liu, K., *Performance of single crystal diamond tools in ductile mode cutting of silicon.* Journal of Materials Processing Technology, 2007. **185**(1-3): p. 24-30.
25. Cheng, K.L., X.;Ward, R.;Holt, R., *Modeling and simulation of the tool wear in nanometric cutting.* Wear, 2003. **255**(7-12): p. 1427-1432.
26. Cai, M.B., X.P. Li, and M. Rahman, *Characteristics of "dynamic hard particles" in nanoscale ductile mode cutting of monocrystalline silicon with diamond tools in relation to tool groove wear.* Wear, 2007. **263**(7-12): p. 1459-1466.
27. Li, X.P., T. He, and M. Rahman, *Tool wear characteristics and their effects on nanoscale ductile mode cutting of silicon wafer.* Wear, 2005. **259**(7-12): p. 1207-1214.
28. Cai, M.B., X.P. Li, and M. Rahman, *Study of the Mechanism of Groove Wear of the Diamond Tool in Nanoscale Ductile Mode Cutting of Monocrystalline Silicon.* Journal of Manufacturing Science and Engineering, 2007. **129**(2): p. 281.

29. Zong, W.J.S., T.;Li, D.;Cheng, K.;Liang, Y. C., *XPS analysis of the groove wearing marks on flank face of diamond tool in nanometric cutting of silicon wafer.* International Journal of Machine Tools and Manufacture, 2008. **48**(15): p. 1678-1687.
30. Goel, S., X. Luo, and R.L. Reuben, *Wear mechanism of diamond tools against single crystal silicon in single point diamond turning process.* Tribology International, 2013. **57**: p. 272-281.
31. Daniel Charles Drucker, W.P., *Soil mechanics and plastic analysis or limit design.* Quarterly of Applied Mathematics, 1952. **10**(2): p. 157-165.
32. Ajjarapu, S.K.P., J. A.;Cherukuri, H.;Brand, C., *Numerical simulations of ductile regime machining of silicon nitride using the Drucker-Prager material model.* Proceedings of the Institution of Mechanical Engineers Part C-Journal of Mechanical Engineering Science, 2004. **218**(6): p. 577-582.
33. G.M.Ohrimenko, *Single crystal silicon piezoelectric ceramics and ferrite under uniaxial compression.* Tranlslated from Problemy Prochonosti, 1988. **9**: p. 45-50.